Development of a flow boiling visualization experiment for liquid hydrogen

Ian Wells[a], Sophia Abi-Saad[a], Thierry Sibilli[b], Jason Hartwig[c], Jacob Leachman[a*]

[a]HYdrogen Properties for Energy Research (HYPER) Center, School of Mechanical and Materials Engineering, Washington State University, Pullman, WA, 99164-2920, USA
[b]Airbus, 21129 Hamburg, Germany
[c]NASA Glenn Research Center, Cleveland, OH, 44135, USA
[*]Email: jacob.leachman@wsu.edu

Abstract. Liquid hydrogen (LH_2) is the highest specific impulse rocket fuel and used on roughly 25% of active United States rocket launch systems. However, these systems are informed by flow boiling heat transfer correlations, the most recent of which has up to 50% root-mean-squared error when used with liquid hydrogen. These errors are exacerbated by the fact that no previous experiments have optically verified multiphase hydrogen flow regimes concurrent with heat transfer measurements. To address this gap, this publication presents the development of a two-phase hydrogen visualization flow cell that can address uncertainty in existing models by providing temperature, velocity, and pressure drop data while identifying flow regimes in two-phase hydrogen. Preliminary results using liquid nitrogen are provided with uncertainties. The resulting system will be used to characterize boiling and heat transfer criticality for increased confidence in multi-phase liquid hydrogen flow estimates for system design.

1. Introduction

Liquid hydrogen (LH_2) is often desired for aerospace cryogenic fuel systems due to its high specific impulse [1], can be sourced from water via electrolysis, and does not emit carbon when reacted. For systems that use gaseous hydrogen (GH_2), fuel is often first stored as LH_2 at near saturation conditions, meaning phase change is present and impacts the size of components for systems like GH_2 turbines and fuel cells. However, designing single-phase LH_2 systems is challenging due to incident heat flux which can evaporate a portion of the fuel unless significant subcooling is present [2]. Therefore, understanding the conditions under which two-phase behavior occurs is necessary to better control and predict performance of LH_2 transfer systems.

Recent numerical models show improved understanding of two-phase hydrogen [3]. However, these works primarily rely on liquid nitrogen testing, have few low mass flux measurements due to the difficulties of flow stratification, and are made using temperature probes external to the flow which increases uncertainty. Flow visualization has also been identified as a key method to improve models via understanding of bubble dynamics, identification of the critical heat flux (CHF) mechanism, and capturing of dominant flow patterns [3]. Additionally, visual data can be made quantitative through recent developments in optical velocimetry techniques. Data for velocity, mass flux, void fraction, quality, and pressure drop can

be obtained using particle image velocimetry (PIV) and used to evaluate existing correlations [4]. To these ends, the Laser Aided Imager for Cryogenic Applications (LAICA) has been developed using in-flow temperature sensors to probe the fluid at the inner surface of a heated wall and use local bubbles as PIV tracers [5].

2. Background

The boiling regimes of a flowing fluid with an externally applied heat flux, shown in *Figure 1*, start with single-phase liquid. Subcooling disappears as heat is added to the fluid. Further heating causes bubbles to nucleate and the fluid enters a two-phase, pre-critical heat flux (Pre-CHF) stage dominated by a liquid phase. Stratified flow can occur at low mass fluxes in this regime. The fluid will reach CHF, which is the maximum amount of heat flux into the system during two-phase flow, following further heating. The CHF point is defined as the location where a liquid film is no longer present on the wall. This triggers one of the two different CHF mechanisms: dryout or departure from nucleate boiling (DNB). Dryout results in dispersed flow film boiling (DFFB) and DNB results in inverted annular film boiling (IAFB). Dryout CHF is associated with low mass velocity and low wall heat flux, characterized by the fluid slowly increasing in vapor fraction, denoted as 'a' in *Figure 1*, as the fluid transitions from fully liquid to fully gas. DNB CHF is associated with high mass velocity and high wall heat flux. IAFB follows after local wall bubbles coalesce into a vapor film which suspends a liquid core in the pipe. The gas fraction of the fluid creates friction against the liquid as more liquid evaporates, causing fluctuations in the core which eventually lead to breakup of the core into slugs and then droplets [6]. At this point, the flow experiences DFFB. With continued heating after DFFB all liquid evaporates, and the fluid is then a single-phase gas.

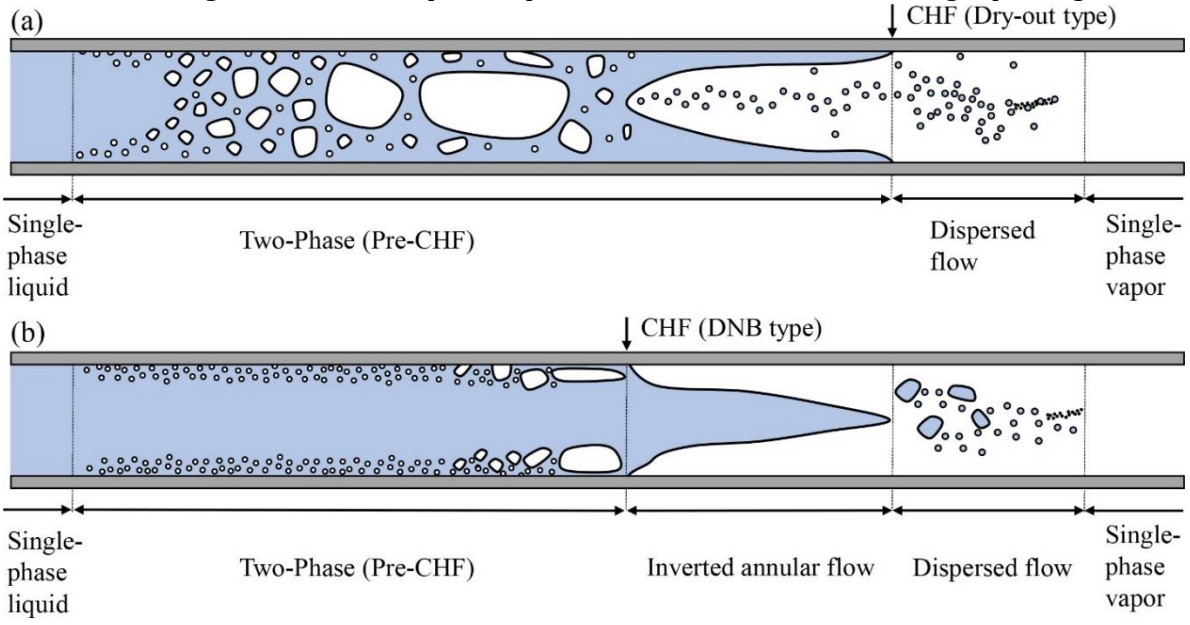

Figure 1*. Boiling regimes for flowing fluid with externally applied heat flux in the (a) Dry-out type CHF case and (b) DNB type CHF case.*

The newest and most accurate correlations to predict two-phase heat transfer coefficient (HTC) and pressure drop in these different boiling regimes are the Purdue University Boiling and Two-phase Laboratory (PU-BTPFL) universal cryogenic flow boiling correlations [3]. These correlations are less erroneous than previous correlations and mark the first time two-phase

hydrogen data has been aggregated in a single unified database. A clear gap that emerged from consolidating all available cryogenic flow boiling data was the lack of visualization to capture dominant flow patterns, bubble dynamics, and the CHF mechanism. These correlations were fit to the widest range of available data, predominately at high mass flux and for horizontal flow. This study tests whether stratified flow is present in addition to providing data to inform further development of these correlations. A summary of relevant past investigations is found in Table 1. The most similar previous work performed by Van Dresar et al [10] involved testing only one heat flux, using a much smaller pipe, no measurement of temperature along the heated section, no internal wall temperature measurement, and 15 Hz imaging. Bronson et al [11] performed chilldown, not heating, experiments and collected images were not published.

Table 1: Comparison of LAICA with previous work.

Source	Maximum Tube ID (cm)	Fluid	Inner Wall Temperature?	Visualization?	Stratified?	Mass Flux (kg-m^{-2}-s^{-1})
Ganesan [3]	1.50	-	No	No	No	4.2-500
Yun et al. [7]	1.07	LN_2	No	No	Yes	58-105
Klimenko et al. [8]	1.88	LN_2	No	No	Yes	60-800
Gao et al. [9]	1.00	LN_2	No	No	Yes	27-71.3
Van Dresar et. al [10]	0.86	LN_2, LH_2	No	Yes	Yes	0.29-34
Bronson et al [11]	11.7	LH_2	No	Yes	Yes	N/A
LAICA (this work)	3.48	LN_2, LH_2	Yes	Yes	Yes	0.1-12.5

3. Flow Cell Design and Experimental Methodology

An experiment was designed to address gaps in the above literature, listed here:

- Local subcooled and saturated boiling HTC for LH_2
- In-flow measurements of inner wall temperature to avoid wall conduction assumptions in calculating the inner wall temperature from the outer wall temperature
- Pressure drop measurements
- Low mass-flux data points (< 20 kg-m^{-2}-s^{-1} for LN_2, < 5 kg-m^{-2}-s^{-1} for LH_2)
- Flow visualization

A diagram of the system is shown in *Figure 2* with photos in *Figure 3*. Instruments and sensitivities are presented in *Table 2*. In LAICA, a 38.1 mm outer diameter, 34.8 mm inner diameter pipe traces a U-shape and is cantilevered from a 1.27 cm thick stainless steel (SS) 304 vacuum chamber lid. This allows the lid to be rolled up to and away from the vacuum chamber without needing to make connections to or from pipes inside the chamber. This also minimizes thermal stresses on the chamber to prevent the need for a metal bellows. The vacuum chamber operates at or below 1 Pa to prevent significant heat influx from the ambient environment and condensation on viewing components. The chamber is a modified compressed air tank with one hemispherical end removed and a 1.27 cm thick SS ring welded to that end. An ethylene propylene diene monomer rubber gasket sits on this face to enable use in non-ultraviolet-protected environments and is coated with vacuum grease to seal against the vacuum chamber lid. The internal diameter of the chamber is 76.2 cm and the wall is 0.5 cm thick SA-414G carbon steel, coated with black polytetrafluoroethylene to reduce surface reflections and oxidation. The outside of the chamber is coated in white Polyester to reflect incident infrared radiation. Conflat ports on the top and side of the chamber are fitted with Ancorp CF450-ZLVP-2.480 Kodial 7056

viewing windows. An NPT-2 port at the back of the chamber allows vacuum to be pulled via roughing pump and vacuum gauges to be mounted.

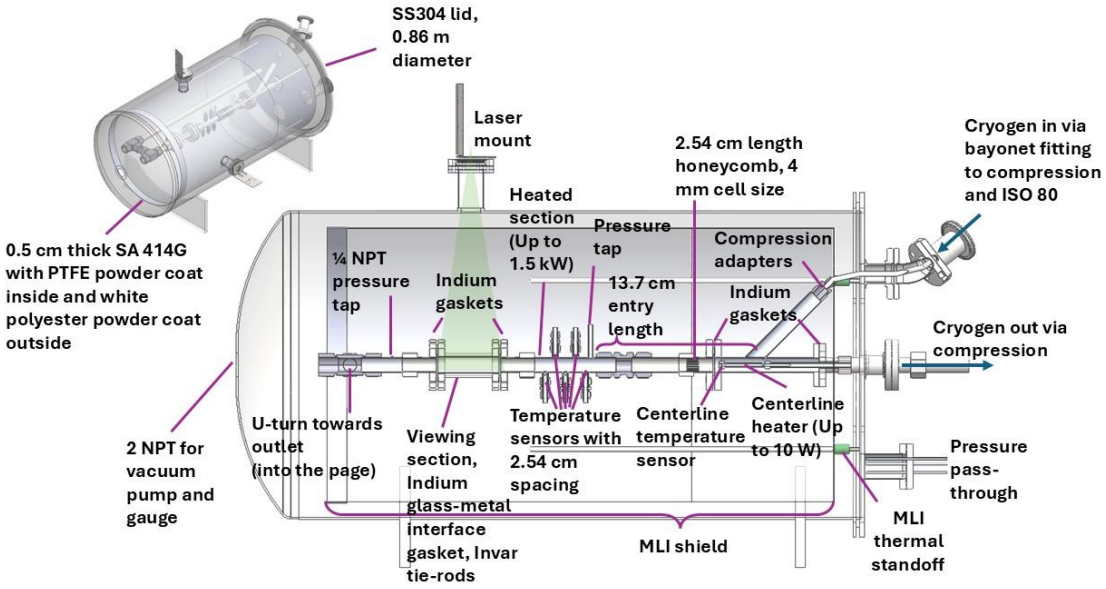

Figure 2: Conceptual diagram of the Laser Aided Imager for Cryogenic Applications (LAICA).

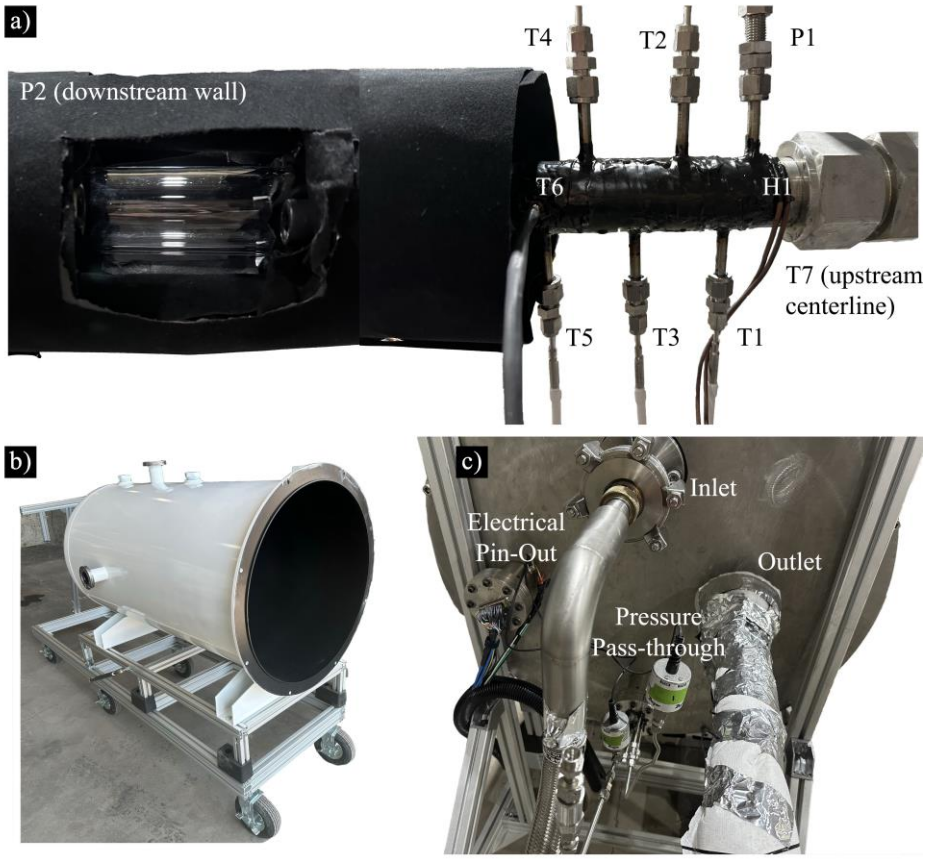

***Figure 3**: LAICA a) viewing glass and thermal manifold with instrument labels and b) vacuum chamber and c) lid with ports labelled.*

***Table 2**: Device and instrument list.*

Instrument	Brand	Model Number	Specifications
T1-T5	Cryotechnics	SD-179A'	±0.15 K at 2-100 K, ±0.25 K at 100-450 K
T6	LakeShore	DT-670A1-CU	±0.25 K at 2-100 K, ±1.5% of temperature at 100-450 K
T7	Scientific Instruments	A424	±0.50 K at 25-400 K
P1, P2	Dwyer	682-2	Range 0-689.5 kPa gauge, 2068 kPa overpressure, ±0.13% F.S. accuracy
H1	-	-	20 gauge Nichrome 80 wire bifilar wound and encased in epoxy, 110 V Variac
W1	Civil Laser	532nm 1000mW Green DPSS Laser	0-0.75 W, Output Wavelength 532±1nm, 30 degree cylindrical lens
W2	Mikrotron Navitar	EoSens2.0MCX12-CM 1-19914	Monochrome, 1920 x 1080 px at 2247 Hz Focal length 50 mm, F/2.0-F/22 adjustable aperture
M1	Alicat	M-2000SLPM-D/5M	±(0.8% of reading + 0.2% of full scale)
D1	LakeShore	218	±200 μV ±0.01% of reading accuracy
D2	National Instruments	NI-9203 input module on an NI cDAQ-9174	16 bit ADC resolution, 200 kS/s maximum sample rate, ±0.49% gain error, ±0.46% offset error

A multi-layer insulation (MLI) shield is used internal to the tank to mitigate radiative heat transfer [12]. The MLI shield has 11 layers of aluminized Mylar, each spaced by Dacron netting. Light reflections internal to the MLI and off the metal components of the sight flow indicator are mitigated by #40 light absorbing black-out material from Edmund Optics. Heat transfer is also mitigated at the entrance to the system via a bayonet fitting from the Mobile Hydrogen Generation unit (MHGU) or a nitrogen dewar used for cryogen supply.

The large pipe diameter is used to slow flows sufficiently for imaging, defined as no more than one pixel of motion between frames at a speed determined by the high-speed camera specifications and the velocity of the fluid assuming homogenous equilibrium flow across the pipe with a quality of 0.1 [13]. Based on the pipe diameter and the fluids of interest (LN_2 and LH_2), an entry length of 13.7 cm was determined to fully develop the flow thermal and hydrodynamic boundary layers assuming turbulent flow and using an upstream thermowell to reduce the thermal entry length [14]. For laminar cases, a honeycomb flow conditioner was placed in the first 2.5 cm of the entry section with a 3.2 mm pore size to maintain a 6-8 pore to length ratio [15]. This produces repeatable flow after at least three times the pipe diameter. A centerline heater is located in the upstream thermowell and can apply up to 10 W of heating. In this thermowell is a silicon diode temperature sensor to evaluate the temperature of the flow entering LAICA.

After conditioning, fluid enters the thermal manifold where the flow is uniformly heated from the outside with up to 1.5 kW via Nichrome 80 wire embedded in Stycast 2850-FT epoxy cured with Cat-24LV catalyst. Along this section, silicon diode temperature sensors T1-T5 are passed through horizontal taps in the wall every 2.54 cm and positioned with the tip of the sensor flush with the wall of the tube to provide fluid measurements at the inner wall without disturbing the flow. T1-T4 are located along the heater and T5 is located just after the heater. T6 is located on the top of the outer wall at the same length along the pipe as T5, enabling a surface temperature measurement on the outside of the pipe. By measuring the four-wire voltage of the nichrome wire

with a voltmeter and using a Hall Effect ammeter, the heating of the pipe can be determined from Ohm's Law for Joule Heating. Then, from the difference in temperature between the fluid at the wall and the fluid upstream at the centerline, the HTC can be calculated from Newton's Law of Cooling. Alternatively, the HTC can be determined based on the wall temperature and the saturation temperature at a measured pressure. Pressure sensors are mounted just before the Nichrome wire and downstream of the visualization section to enable two-phase pressure drop measurement. These can also be connected to a differential pressure transducer.

Following heating, the cryogenic flow enters a viewing glass. To ensure sufficient illumination, a 0.75 W power-tunable 532 nm diode pumped solid state laser illuminates the flow. The laser, which produces a continuous beam, was outfitted with a cylindrical lens to produce a laser sheet. A GentecEO XLP12-3S-H2-INT-D0 NIST calibrated laser power meter was used to verify the specifications of the laser system. Hydrogen flows can be supplied at mass flow rates up to 5 g/s by MHGU [16] and nitrogen flows can be supplied at the maximum mass flow rate out of a 160 L low pressure dewar. The influence of para-orthohydrogen conversion on lighting is minimal, in line with previous experiments [17], due to the lack of activated catalyst material and the low equilibrium orthohydrogen fraction at the temperatures of interest [18]. The viewing glass is a modified Archon Industries AKGF015-C31A001 full-view sight flow indicator. The off-the-shelf (OTS) part is a borosilicate sight glass with a length of 15.2 cm compressed against NPS 1-1/2 ANSI 150 flanges by tie rods with Gylon seats. The OTS component was modified to use Invar 36 tie rods, 2 mm thick indium gaskets on sealing surfaces, and Belleville washers to ensure leak tightness below a 3.2E-7 sccs helium leak rate reliably, even with cryogenic cycling.

To investigate the impact of gravity on flow characteristics, the vacuum chamber sits on an aluminum strut frame which can be tilted and locked in place at angles between horizontal and vertical orientation. This frame is mounted on casters for transport between test locations. Optical data is stored on a dedicated computer. Temperature data is stored on another computer after passing through a LakeShore 218 temperature controller and being recorded in LakeShore Chart Recorder. Pressure and mass flow rate are imported through an NI-9203 input module on an NI cDAQ-9174 system into LABVIEW. Optical data is correlated to temperature, pressure, and mass flow by the internal clock time attached to all images. Times are matched between the optical data and the thermophysical measurements with timing accuracy determined by the drift in the internal computer clock between the two devices.

4. Results and Discussion

Results of flow boiling tests with LN_2 are presented here for verification of results before testing with LH_2, and for contribution of low mass flux LN_2 data to the flow boiling literature. At the low flow rates used, the system experienced optically verified stratified or intermittent flow in all tested conditions. This stratified flow condition led to much lower critical heat flux values, as shown in other previous work [19], than predicted by the universal correlations with 14 steady state points tabulated in *Table 3*, a pre-CHF and post-CHF image shown in *Figure 4*, and a comparison between the correlations and experiment steady state HTC in *Figure 5*. In this comparison, the regions of HTC associated with pre-CHF and post-CHF modes, as predicted by the correlations, are shaded. The experiment data is marked as pre-CHF or post-CHF, with post-CHF* indicating an oscillation between pre-CHF and post-CHF behavior at the temperature sensor. A 1:1 line marks hypothetical correlation-experiment agreement. Although the correlations apply to some of the tested mass fluxes, due to omission of stratified and intermittent boiling regimes in the correlations a fair comparison cannot be made. The Mean Absolute Percent Error (MAPE) was 214.5% with error increasing as heat flux increased. The data in *Table 3* is equal to the average

over one minute at a steady state point, defined when no more than ±0.5 K variation occurs in temperature over the same minute. Variation is equal to either the standard deviation over the steady-state point or the sensor error, whichever is greater. Based on a boil-off test measuring the exiting mass flow rate with the inlet closed and the system tilted such that only vapor could exit the chamber, heat leak over all internal pipes was 3.66 W. Of note are droplets sometimes visible on the surface of stratified flow, which appear undocumented in cryogenic flow boiling.

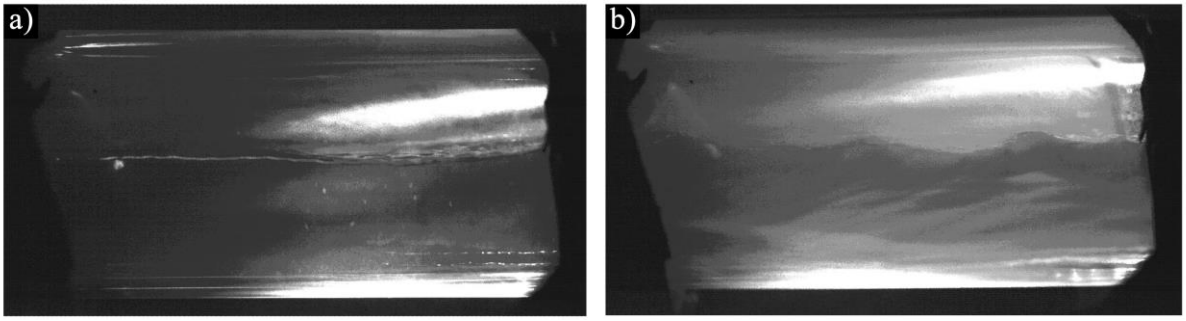

***Figure 4**: Comparison of a) pre-CHF and b) post-CHF flow at mass flux = 4.477* kg-m^{-2}-s^{-1}.

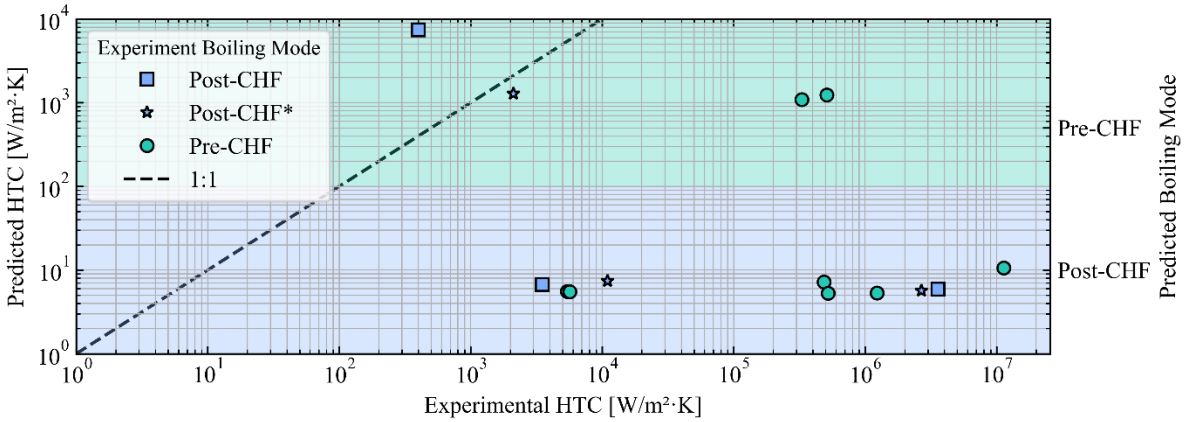

Figure 5: Steady state measured heat transfer coefficient compared with predicted values from the PU-BTPFL correlation. Boiling modes are also compared with "Post-CHF*" indicating oscillation between pre-CHF and post-CHF behavior.

***Table 3**: Pre-CHF, at-CHF, and post-CHF data points of interest from testing with LAICA.*

Heat Flux (kW-m^{-2})	T4 (K)	T5 (K)	T6 (K)	T7 (K)	P1 (kPa)	Mass Flux (kg-m^{-2}-s^{-1})
11.08	83.98±0.15	83.80±0.15	177.13±0.25	84.38±0.50	214.6±0.9	2.634±0.042
12.10	129.06±0.46	112.17±0.25	189.60±0.25	83.78±0.50	214.4±0.9	2.623±0.042
11.86	293.40±0.25	171.06±0.20	276.56±0.25	83.95±0.50	216.0±0.9	2.107±0.042
5.63	84.13±0.15	83.93±0.15	119.68±0.47	83.81±0.50	217.4±0.8	2.104±0.042
6.80	84.05±0.15	117.22±0.25	148.07±0.25	84.95±0.50	216.4±0.9	2.107±0.042
6.82	103.01±0.25	114.95±0.25	156.90±0.25	83.95±0.50	216.4±0.8	3.075±0.042
1.88	84.10±0.15	83.91±0.15	113.65±0.25	84.06±0.50	217.0±0.8	1.590±0.042
2.08	84.10±0.15	83.96±0.15	117.07±0.25	84.06±0.50	217.2±0.8	1.570±0.042

2.21	92.00±0.23	111.02±0.25	120.83±0.25	84.06±0.50	216.4±0.7	1.588±0.042
6.11	83.52±0.15	83.26±0.15	117.60±0.25	83.56±0.50	201.0±1.2	2.055±0.042
8.57	146.62±0.29	82.95±0.15	171.69±0.25	83.01±0.50	196.1±1.1	2.118±0.042
7.76	116.59±0.39	82.81±0.15	159.77±0.25	82.89±0.50	192.9±0.8	2.074±0.042
18.19	82.72±0.15	82.51±0.15	179.29±0.25	82.55±0.50	186.4±1.5	4.477±0.543
0.43	106.30±0.26	113.05±0.25	-	85.34±0.50	243.5±1.2	0.218±0.042

5. Conclusion

The above testing documents and evaluates a flow boiling visualization system for LN_2 and LH_2. Initial results identify the point of CHF for LN_2 at multiple mass fluxes. Stratified and intermittent flow were visually observed at mass fluxes where literature correlations predict nucleate boiling. A mean absolute percent error of 214.5% was found between experimental and predicted heat transfer coefficients. This large discrepancy highlights the need for further studies to investigate gravitational and mass flux effects for improving models of cryogenic flow boiling and boiling regime maps, particularly at low mass flux conditions.

Acknowledgements

The results of this work were supported by a NASA Space Technology Graduate Research Opportunity grant #80NSSC24K1357 and LAICA was developed in collaboration with Airbus.

References

[1] I F Silvera and J W Cole 2010 *J. of Phys.* **215** 012194 [10.1088/1742-6596/215/1/012194]
[2] J Zhang, T S Fisher, P V Ramachandran, J P Gore, and I Mudawar 2005 *J. Heat Transfer* **127(12)** pp 1391–1399 [10.1115/1.2098875.]
[3] V Ganesan, 2023 *PhD Thesis* Purdue University, West Lafayette
[4] J Ortega, G Anaya, C Ho, P Vorobieff, and G Mohan 2023 *J. Sol. Energy Eng.* **145(4)** 041007 [10.1115/1.4054358]
[5] M Kim, J H Lee, and H Park 2016 *Exp. Fluids* **57**, 55 [10.1007/s00348-016-2144-6]
[6] Q Liu, J Kelly, and X Sun 2021 *Nuclear Eng. Design* **375** 111082 [10.1016/j.nucengdes.2021.111082]
[7] R. Yun, J Hwang, J T Chung, Y Kim 2007 *Int. J. Heat Mass Transfer* **50(11-12)** 2339-2345 [10.1016/j.ijheatmasstransfer.2006.10.038]
[8] V V Klimenko, M V Fyodorov, Y A Fomichyov 1989 *Cryogenics* **29(1)** 31-36 [10.1016/0011-2275(89)90008-8]
[9] Y Gao, Z Wang, Y Li, E Ma, H Yu 2024 *Int. J. Heat Fluid Flow* **107** 109335 [10.1016/j.ijheatfluidflow.2024.109335]
[10] N T Van Dresar, J D Siegwarth, M M Hasan 2001 *Cryogenics* **41(11-12)** 805-811 [10.1016/S0011-2275(01)00173-4]
[11] J C Bronson, F J Edeskuty, J H Fretwell, E F Hammel, W E Keller, K L Meier, A F Schuch, W L Willis 1962 **7** [10.1007/978-1-4757-0531-7_25]
[12] R. G. Ross 2015 *IOP Conf. Ser.: Mater. Sci. Eng.* **101** 012017 [10.1088/1757-899X/101/1/012017]
[13] M. Versluis 2013 *Exp. Fluids* **54** 1458 [10.1007/s00348-013-1458-x]
[14] G Nellis and S Klein 2009 *Heat Transfer* (Cambridge University Press)
[15] J Scheiman 1981 *NTRS* NASA-TM-19810020599
[16] Y K Gitter and J W Leachman 2024 *IOP Conf. Ser.: Mater. Sci. Eng.* **1301** 012064 [10.1088/1757-899X/1301/1/012064]
[17] R C Hendricks, R W Graham, Y Y Hsu, and R Friedman 1961 *DTIC* AD0255524
[18] J Leachman, R T Jacobsen, S G Penoncello, and E W Lemmon 2009 *J. Phys. Chem. Ref. Data* **38** 721–748 [10.1063/1.3160306]

[19] C R Kharangate, L E O'Neill, I Mudawar, M M Hasan, H K Nahra, R Balasubramaniam, N R Hall, A m Macner, J R Mackey 2015 *Int. J. Heat Mass Transfer* **90** 323-338 [10.1016/j.ijheatmasstransfer.2015.06.073]